CFD Simulation of Flow in Vortex Diodes

A. A. Kulkarni and V. V. Ranade
Industrial Flow Modeling Group, National Chemical Laboratory, Pune - 411 008, India

R. Rajeev and S. B. Koganti
Indira Gandhi Center for Atomic Research, Kalpakkam - 603 102, India

DOI 10.1002/aic.11439
Published online March 17, 2008 in Wiley InterScience (www.interscience.wiley.com).

Vortex diodes are used as leaky nonreturn valves in applications, where it is desirable to avoid valves with moving parts. Despite their use in practice for several decades, no detailed analysis of the flow inside the vortex diodes is available. A strategy was derived for the CFD simulations of the vortical flow in diodes. A good agreement was seen between pressure drop (ΔP) across the inlet-outlet ports from CFD simulations, and the experimental data for five diode sizes. The simulations showed that in the reverse flow situation tangential velocity was dominant and resulted in conservation of angular momentum in the chamber until it reaches the axial exit port. This vortical motion induced a significant pressure drop (ΔP_r). The axial velocity gradient over the chamber cross-section helps in inducing relaminarization of the flow. In the forward flow mode, the fluid gets distributed radially over the chamber and exits through the tangential port, yielding low ΔP_f. The analysis showed that the performance of a diode is strongly affected by diode geometry, size, aspect ratio, nozzle configuration and Reynolds number. Among different configurations, the nozzles with entry port size equal to diode yielded higher diodicity. Simulations showed that using angle of divergence for diffuser sections of nozzles of the order of 7° exhibited higher diodicity than smaller angles. It was also observed that at higher flow rates significantly higher diodicity was obtained using axial nozzles with larger radius of curvature for expander section. The modeling methodology and results presented will be useful for evolving better designs of vortex diodes.
AIChE J, 54: 1139–1152, 2008
Keywords: vortex diode, CFD, diodicity, pressure drop, relaminarization

Introduction

Fluidic systems like vortex tube,[1–3] cyclone separators,[4–6] swirl tube,[7] hydrocyclones,[8] vortex whistle, swirl combustors,[9] and the vortex diode,[10–12] are widely used in various engineering applications. The performance of these devices is largely dominated by the confined turbulent vortex/vortices, due to the tangentially entering fluid. Usually such devices have a large-scale swirl component and often show counterintuitive effects on the flow field like periodic vortex core precession, development of a subcritical flow, due to the downstream conditions on the entire flow, and vortex breakdown. Predictive models and methods for simulating swirling flows in such devices are of great practical value for evolving optimum designs. In this manuscript we focus on understanding flow inside the vortex diode using CFD models.

Correspondence concerning this article should be addressed to V. Ranade at vv.ranade@ncl.res.in.

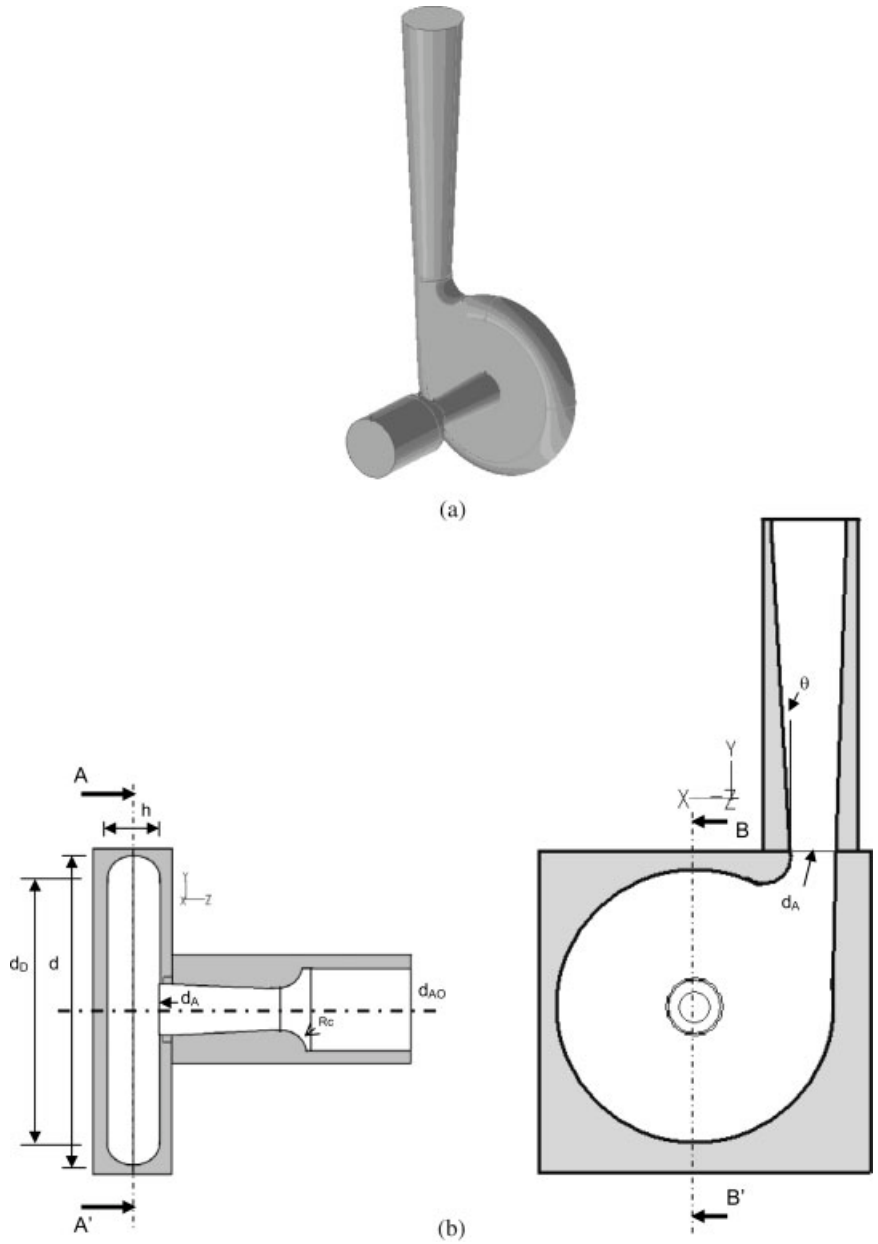

Figure 1. (a) Diode used in this work, and (b) cross-sectional views of a 150 mm vortex diode.

The basic design of a vortex diode consists of a disc-shaped chamber with cylindrical axial and tangential ports (Zobel,[13] this point onward this basic design will be referred as Zobel diode). Typical diode used in this work is shown in Figure 1A. Unlike the basic diode design proposed by Zobel,[13] the diode used in this analysis has the following differences: (1) the tangential nozzle is a single diffuser section (2) the tangential nozzle is attached to the chamber in a smooth manner without generating obstructions in the flow path, (3) the axial nozzle is made of three sections, a short diffuser section, an expander and a straight section, and (4) the total divergence angle of the diffuser section for both axial, as well as tangential nozzles are identical. The flow entering the device through the tangential port sets up a vortex, and establishes a large pressure drop across the device. On the other hand, when fluid enters through the axial port it creates a substantial radial flow distribution over the chamber cross-section and develops only a modest pressure drop. Vortex diodes find applications in nuclear industry as a leaky nonreturn valve and in hydraulic/thermal power stations, mainly to dampen the oscillations in pipe systems.[14] In most of the applications it is used in combination with other fluidic devices. The performance of a vortex diode is measured in terms of diodicity D, defined as the ratio of reverse flow pressure drop to the forward flow pressure drop for the same inlet flow rate i.e., $D = \Delta P_r/\Delta P_f$. The terms reverse and forward correspond to the undesired (tangential to axial nozzle), and desired (axial to tangential nozzle) direction of flow,

respectively. The design of the vortex diode is made such that the diodicity is as high as possible.

The concept of vortex diode is not new. In one of the earliest detailed investigations, Zobel[13] has done a significant work on the optimization of a specific design of vortex diode. His analysis was based on the performance of a diode for a wide range of chamber aspect ratio ($\alpha = d/h$), diode diameter, length of inlet ports, etc. However his designs achieved relatively low-values of diodicity,[10] and efforts were made to further improve the design. Priestman and Tippetts[12] and Priestman[10,11] carried out systematic experiments and viscid flow analysis of vortex throttles. His experimental data (from different diode sizes, different aspect ratio, nozzle designs and nozzle configurations) showed that in the absence of wall friction, the strength of the vortex formed increased with increasing chamber diameter. He also observed that the inception of cavitation reduces the pressure drop across the diode. From the analysis based on the viscid flow in the diode chamber, he showed that at higher Reynolds number ($Re = d_A v_A \rho/\mu$, where d_A is the diameter of the portion of nozzle attached to the chamber, and v_A is the corresponding flow velocity. ρ and μ are fluid density and viscosity, respectively), optimum performance of a diode is achieved at an aspect ratio of 6, while for lower Re, it was smaller.

Although these prior analyses helped in some way to find the ways to optimize some of the diode design parameters, it was clear that the knowledge about the flow pattern inside the diode would help in designing better systems. In the diode chamber, the vortical flow can be clearly divided in two segments, i.e., free vortex and forced vortex (Figure 3 of Stairmand[15]). In view of this, Stairmond[15] developed an analytical method for identifying the region of transition of the nature of vortex in the chamber using analytical approach and verified it using computational fluid dynamics. Similar to Wormley,[16] he defined a term, modified boundary layer coefficient (BLC*) as; $\mathrm{BLC}^* = 2\alpha f S/\mathrm{Re}^{0.25}$, with $\mathrm{Re} = \upsilon_i h/2\nu$, where υ_i is the radial fluid velocity at $r = R$, h is the chamber height, and ν is the kinematic viscosity According to his analysis, for $\mathrm{BLC}^* \leq 0.25$, the circulation in the chamber is conserved. With increasing BLC*, the region of the forced vortex increases until the value is close to $\mathrm{BLC}^* \sim 2$, at which it occupies most of the chamber. For such a case, angular momentum is not conserved, and the swirl velocity either remains constant or decreases. Based on the viscid flow analysis, he proposed the nature of pressure profile in the chamber indicating that in the inertial range, the pressure values inside the chamber are independent of chamber aspect ratio i.e., α. He verified his propositions by using the numerical analysis of the flow in the chamber, and showed that the velocity profile assumed by Wormley[16] was not fully correct.

This brief overview of the published literature indicates that detailed understanding of flow inside the diode chamber and specific guidelines for the optimum design of diodes are not available. It is obvious that the best design of diode would aim at setting-up a stronger vortical flow in reverse flow, and better uniform radial distribution of fluid in forward flow. The aforementioned two conditions can be achieved if two important (among several) complexities in the flow in the chamber i.e., (1) the characteristics of vortex formed in reverse flow mode, and (2) uniformity in the radial distribution of fluid in the forward flow situation are understood. In the diode chamber, the swirl component of the vortical flow increases from the periphery toward the center. This increment occurs only till a critical radius (i.e., transition of nature of vortex), after which the tangential velocity becomes linearly proportional to the radius itself. In other words, in the free vortex region, the value of the product $w \cdot r$ is almost constant until the chamber periphery, while in the forced vortex region w/r is more or less constant. The characteristics of such a centripetal vortex in the chamber is strongly decided by the dynamics of the forced vortex region, the nature of vortex transition and the diode design itself. However, the implications of the regions occupied by the forced and free vortices on optimizing the performance of a diode are still not clear. Secondly, the contribution of pressure drop in forward flow (ΔP_f), is quite important because it appears at the denominator in the definition of diodicity. The more uniform radial distribution in the forward flow would yield lower ΔP_f and higher diodicity.

In light of this brief review, we have carried out CFD simulations to understand the flow characteristics of vortex diode and to quantify influence of various design parameters on its performance. In the section of CFD model, the boundary conditions, their implementation in FLUENT and parameters used during the simulations are discussed in detail. For the model equations, reader is referred to suitable references. The predicted results were compared with the experimental data obtained for a range of diode sizes. This was followed by the discussion on key features of flow in vortex diodes and influence of design parameters on flow and diode performance. In the last section, conclusions of this work are highlighted.

CFD Model

Flow in vortex diode exhibits complex characteristics as indicated by brief literature review discussed previously. Unlike simple flows, there are more than one characteristic length and velocity scales associated with flow in diodes. This complicates the task of defining characteristic Reynolds number of the flow in vortex diodes. In this work, as indicated previously, the Reynolds number is defined based on a velocity at the location where the axial or tangential port attached to the diode chamber. For the range of Reynolds number considered in this work, the flow in inlet pipe is turbulent. However, when the flow enters through axial nozzle in the diode chamber, the characteristic velocity reduces significantly and flow may become laminar. In case of entry through tangential nozzle, a strong vertical flow sets-up. Such vertical flows are known to undergo a relaminarization process. The strong swirling flow experiences a preferential stretching in tangential direction which may damp fluctuations (turbulence). Ragab and Sreedhar[17] have discussed the relaminarization mechanism in terms of the combined effect of strength of axial velocity gradient, and the magnitude of swirling flow. The axial velocity gradient in the chamber is important due to its role in the extraction of energy from the mean flow to continue the energy transfer and the dissipation. In the diode chamber the axial velocity component loses its dominance, and, thus, breaks the cascade process. This may result in the relaminarization of the flow.

Table 1. Geometrical Details of the Diodes Studied Experimentally (Notations refer to Figure 1b)

Diode chamber		Details about nozzle design			
Diameter d (mm)	Height h (mm)	Axial nozzle $d_A-d_E-d_{AO}$(mm)	R_C (mm)	Tangential nozzle d_T-d_{TO} (mm)	θ (degree)
25, 30	6	6–4–9.5	16	6–9.5	5
45, 55	9	9–6–15.7	16	9–15.7	5
60, 70, 80, 90	15	15–12–26.7	16	15–26.7	5
100, 125, 150	25	25–20–40.9	16	25–40.9	5
		20–16–40.9		20–40.9	

The transition from turbulent flow in inlet pipe to laminar flow in diode chamber will require some space and ideally a direct numerical simulation[18] of flows will provide detailed understanding of laminarization of flows in vortex diodes. However, the resources required to carry out full DNS were not available to us. Besides this, the aim of this work was to understand influence of various design parameters on performance of vortex diodes, which required relatively quick simulation methods. In absence of the ability to carry out DNS simulations, we used RANS approach to simulate flow in vortex diodes. Preliminary simulations were, therefore, carried out with the standard k-ε turbulence model. However, the simulated results (briefly discussed later) showed significant deviation from the experimental data. Considering the possibility of relaminarization, we have, therefore, omitted Reynolds stresses and replaced turbulent viscosity by molecular viscosity. This approach is not rigorously valid near the entrance region since the flow at the inlet pipe is turbulent. However, the simulated pressure drop and diodicity values based on this approach appeared to be closer to the experimental data than those obtained with the two equation turbulence model. All the subsequent simulations of flow in vortex diodes were, therefore, carried out without any turbulence model. Steady as well as unsteady simulations were carried out to identify possibility of unsteady flow especially in cases with tangential entry. The standard Navier-Stokes equations (and Reynolds averaged version for the turbulent simulations) were used in this work. These equations are not presented here for the sake of brevity and may be found in for example, Ranade.[19] The considered geometry, boundary conditions used in this work and solution method are discussed later.

Geometry of diodes, boundary conditions and solution method

Typical geometry of vortex diodes considered in this work is shown in Figure 1B. Characteristic dimensions of the diodes considered in this work are listed in Table 1. The boundary conditions used in this work are also indicated in Figure 2. The inlet boundary condition was defined as "velocity inlet" and the value of fluid velocity (and turbulence intensity and hydraulic diameter for turbulent simulations) at the inlet was given as the inlet boundary condition. The outlet boundary condition was defined as "constant pressure outlet," and the outlet pressure was specified as zero (relative to the operating pressure). However, our initial simulations indicated circulating flow at the outlet (when fluid entered through tangential inlet). Such circulatory flow causes distribution of pressure at the outlet and may result in the reverse flow from the outlet. To avoid reverse flow, and to ensure the constant pressure boundary condition at the outlet, additional resistance at the outlet was specified (using the "outlet vent" boundary condition of FLUENT). The value of the loss coefficient was gradually increased to avoid reverse flow from the outlet. The pressure loss at the outlet was not included while reporting the pressure drop across vortex diodes. The predicted pressure drop values were seen to be insensitive to further increase in the loss coefficient.

The diode geometry was modeled using GAMBIT (of FLUENT Inc., USA). Different sets of computational grids were developed to understand influence of grid size on predicted results. Typical computational domain and the sectional view of the computational grids are shown in Figure 2. Diode geometry was meshed using either hexahedral elements or tetrahedral elements, or a combination of both, depending on the complexity of the domain. The model equations were solved using FLUENT 6.2 (of Fluent Inc., USA). SIMPLE algorithm was used for pressure and velocity coupling and equations for flow simulation were solved. Water was used as a fluid flowing through vortex diode. Pressure based solver was chosen with implicit formulation, suitable gradient option (cell/node).

In order to examine possibility of unsteady nature of the flow in vortex diodes when liquid is fed via tangential inlet, the flow inside a 125mm diode at inlet fluid velocity of 0.55 m/s was simulated using steady, as well as unsteady solver. Initially we performed the steady-state simulations (with a set of parameters, discussed in the next subsection) and estimated the pressure drop across the diode, and also monitored the pressure variation at two ports, and the flow profiles inside the chamber. It was observed that the simulated pressure drop for the reverse flow mode oscillated continuously in a range. Moreover, the tangential velocity profiles inside the chamber showed that the center of the vortex did not match with the geometrical center of the chamber. The average pressure drop over a large number of iterations was estimated and used for calculating the respective Euler number ($Eu = \frac{2\Delta p}{\rho v_A^2}$, where v_A is the velocity at the port connected to the diode chamber with diameter d_A) for reverse flow (Eu_r = 68.87), and forward flow (Eu_f = 1.426), and, hence, the diodicity (48.29). Further, we also carried out the unsteady simulations of the flow in the diode, and monitored the aforementioned parameters in time. After the steady-state simulations, the unsteady simulations were carried out with a time step of 0.005s and 30 iterations per time step, and

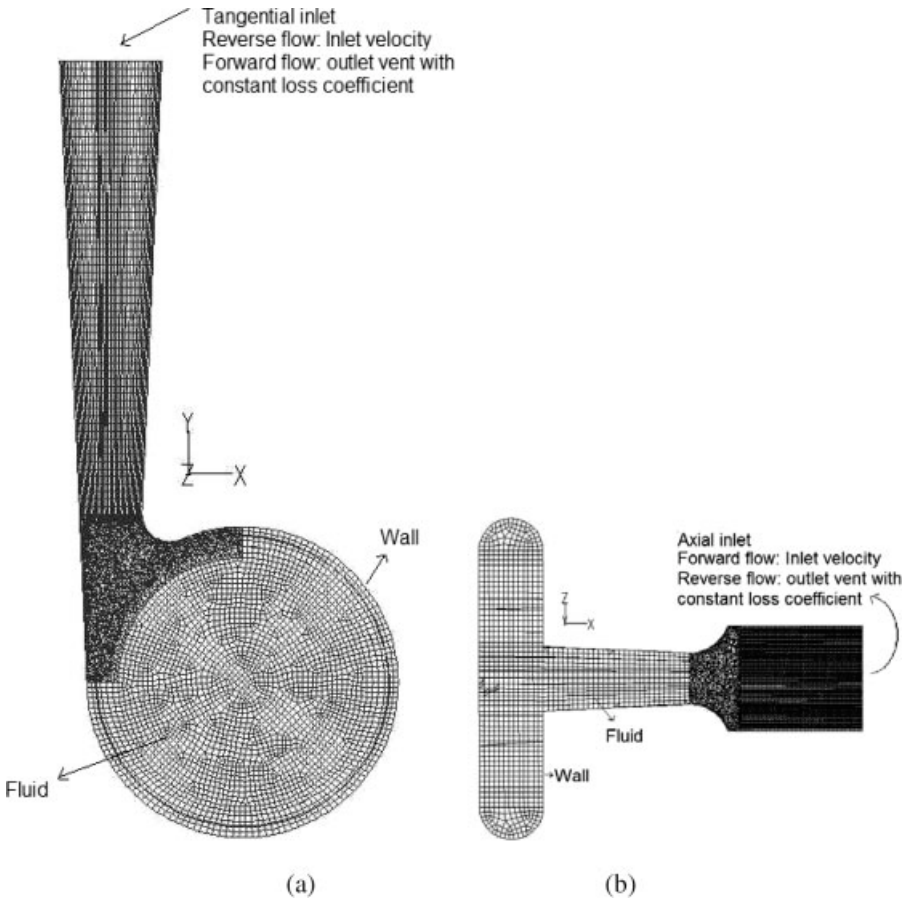

Figure 2. Computational domain and the boundary conditions of the vortex diode (a) sectional view in the XY plane, and (b) sectional view of the XZ plane.

pressure at the inlet and outlet were monitored in time. The results showed that for the case of reverse flow simulations, the pressure at the tangential inlet oscillated continuously in a narrow range. Again, the averaged values of pressure drop were used for estimating the reverse flow, as well as forward flow *Eu* (68.2 and 1.43, respectively), and also the diodicity (49.01). The simulations showed that the range of pressure drop variation observed for steady and unsteady simulations (for both, reverse flow, as well as the forward flow) were very close (+2.3%), which yielded relatively close values of the diodicity. Second, the tangential velocity profiles over the chamber cross-section obtained at different time steps were plotted along with the profiles from steady-state simulations (Figure 3). It can be seen that the profiles from the steady-state simulations fall in the range of profiles obtained by unsteady simulations. Moreover, in both cases, the center of the vortex deviates from the geometrical center with similar magnitude (2 to 5 mm). These similarities in the results indicate that the steady-state simulations may be used to understand the influence of key design and operating parameters on diode performance. All the subsequent simulations for this purpose were, therefore, carried out with steady solver. The predicted results based on steady-state simulations are discussed in the next section.

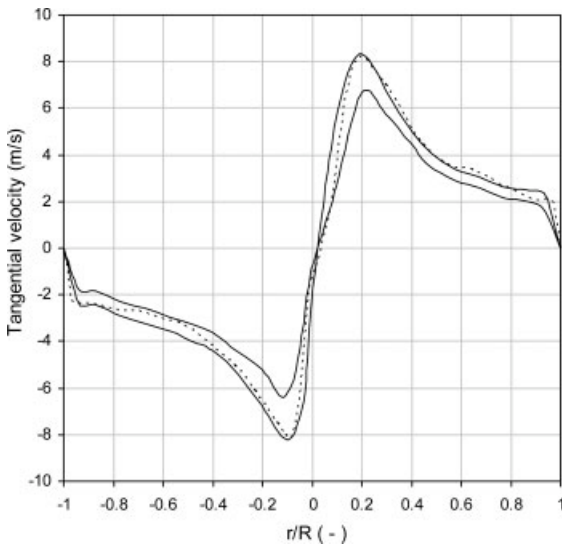

Figure 3. Tangential velocity profiles over the chamber cross-section.

The solid lines show the range of values of the tangential velocity that can be seen from the unsteady simulations. The dotted line shows the tangential velocity profile obtained from steady-state simulations.

Results and Discussions

Selection of simulation parameters

In the first set of simulations, the numerical experiments were carried out to select appropriate boundary conditions and numerical parameters like (1) discretization scheme for pressure and momentum equations, (2) number of grids, and (3) under-relaxation parameters, etc. The details of the selection are discussed following.

Effect of Inlet Boundary Condition. In all the simulations, area weighted average pressure was monitored at the two boundaries (axial and tangential port). In order to check the effect of type of inlet boundary condition, the simulations were carried out for 90 mm diode (inlet flow rate ~200 LPH) by providing (1) a flat velocity condition, and (2) one seventh law velocity profile $\left[V = V_{\max}(1 - r/R)^{1/7}\right]$ at the inlet boundary. The difference in the average pressure-drop obtained for the two cases was not significant (<3.2%), and was within experimental error. Moreover, the mean velocity profiles in the chamber for the two cases were similar, and, hence, for further simulations we used a flat inlet boundary condition.

After deciding the suitable boundary conditions, influence of grid size, grid type and the discretization scheme was examined. Since the use of most desirable hexahedral grids for the entire geometry was difficult due to the complexities in certain regions of the geometry, a combination of hexahedral and tetrahedral grids was used. In most of the cases, the region of chamber where it is attached to the tangential port was meshed with tetrahedral grids, while mesh for the remaining sections of the diode geometry (i.e., remaining three quarters of the chamber, tangential port, converging section at the axial entry, expander at the axial port, etc.) was hexahedral. A case of a 125 mm diode (with the inlet velocity of 0.55 m/s for reverse flow, as well as the forward flow situations) was considered to carry out numerical experiments for selecting the appropriate simulation parameters.

Effect of Grid-Size and Discretization Schemes. Three grid sizes (1×10^5, 3×10^5 and 10×10^5 computational cells), and two momentum discretization schemes (second-order upwind and MUSCL, see FLUENT documentation for more details) were considered for this analysis. The predicted results are shown in Figure 4. It can be seen that the variation in the predicted diodicity was less than 1% for more than 300,000 computational cells. All the further simulations were carried out using a minimum 300,000 computational cells. The simulations with hexahedral and tetrahedral cells showed similar results. The difference in the pressure drop for simulations with geometry having hexahedral cells, and the tetrahedral cells was less than $\pm 0.3\%$ for the reverse flow operation of a diode. For the case of forward flow operation, this difference was less than $\pm 0.1\%$. In further simulations, hexahedral mesh was used for the cylindrical portion of the chamber and the inlet ports. In the region where the tangential port is attached to the chamber, the tetrahedral meshing was employed. The predicted results did not show any significant difference between second-order upwind and MUSCL discretization schemes. Therefore, for all the subsequent simulations the second-order upwind scheme was selected for discretization of momentum equations.

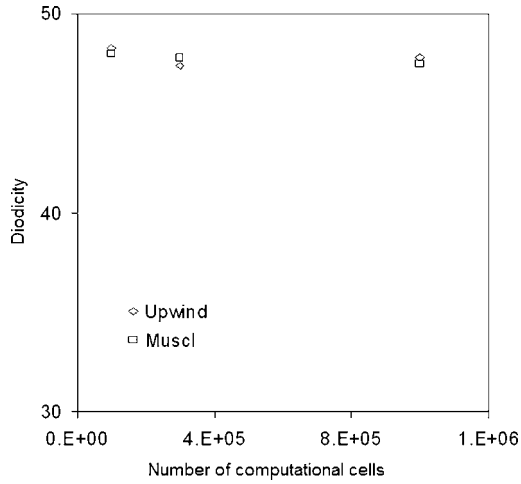

Figure 4. Effect of number of computational cells on the simulated diodicity for two different simulation schemes, 125 mm diode at inlet velocity of 0.5497 m/s.

Discretization of pressure equation is also important especially in case of strongly swirling flows. Recently, Muntean et al.[20] and Susan-Resiga[21] have used PRESTO! discretization scheme for pressure equation, for simulating swirling flow in tubes. Unlike these systems, the flow in vortex diodes is not symmetric. In diodes, though a free vortex region exists, the axial port attached to the chamber causes the central region to behave as a forced vortex. More importantly, the aforementioned two studies considered systems with higher aspect ratio, and it is not clear whether their recommendations will hold for vortex diodes. Simulations were, therefore, carried out with the standard and PRESTO! (PREssure STaggering Option) schemes for discretizing pressure (see FLUENT user manual and references cited, therein, for more details of these discretization schemes), and results were compared with the experimental data. Standard scheme interpolates the pressure values at the faces using momentum equation coefficients. For flows with high-swirl numbers, high-speed rotating flows, and flows in strongly curved domains, usually PRESTO! scheme is used. Our simulations showed that the PRESTO! scheme always yielded higher pressure-drop for the case of reverse flow, while the forward flow pressure-drop was similar to that of the standard scheme. Importantly, the simulations using PRESTO! required significantly more iterations to obtain converged solution compared to the standard scheme. The simulations using PRESTO! converged after relatively very large number of iterations at a value close to 21.4% higher than the converged result predicted by the standard discretization. For understanding the possible reason behind the significant difference in the simulations using PRESTO! it would be worthwhile to have experimental data of internal velocity variation. Second, from the simulations at higher velocities for the same diode, higher pressure-drop yielded larger pressure and velocity gradients toward the center of the chamber. Which means that the simulations from PRESTO!, which also yield larger velocity and pressure gradients does not

appropriately take into account the region of forced vortex. These analyses were repeated for two inlet velocities, and the observations were consistent. In view of this and in absence of data on velocity profiles within diodes, it was decided to carry out the subsequent simulations using the standard pressure discretization scheme.

Few simulations were also carried out to evaluate influence of cell based and node based gradient calculations. The simulations for 150mm diode for 0.55 m/s inlet velocities showed that the forward, as well as reverse flow pressure drop values from both the gradient options were not very different (<3.6%). Based on this, cell based gradient option was used in all the further simulations.

Before, we discussed the details of simulated flow in vortex diodes, a brief discussion on comparison of results predicted with the assumption of laminar and turbulent flow in the chamber is given here. Flow in vortex diode of 90 mm dia. was simulated with and without the two equation k-ε turbulence model, based on RANS equations over a range of Re at the tangential port (4,700–28,000).[22] The simulations showed that the pressure-drop values predicted using the k-ε model, were less than the experimental data (see Figure 5A). The reason behind the difference may be justified as: the hydraulic diameter of the chamber is much greater than the diameter at the tangential port. As indicated earlier, the value of chamber Re (Re_{ch}) is much smaller than the Re at inlet port, and, hence, the possibility of the flow remaining turbulent is less. The stretching of the fluid in one direction along the tangential direction may lead to laminarization of the flow. The strong swirling flow combined with a weak axial velocity deficit (difference in the axial velocity of vortex edge and core) leads to stable vortex and relaminarization.[17,23–25] For the forward flow, the comparison of the predicted pressure drop with the standard k-ε model, and the laminar flow model is shown in Figure 5B. It can be seen that even in the case of forward flow, the predicted pressure-drop values by assuming the laminar flow are closer to the experimental data than those predicted by the k-ε model, though the difference is less than that observed in the case of reverse flow. Based on these results for all the subsequent simulations, flow in vortex diodes was assumed to be laminar and no turbulence model was used.

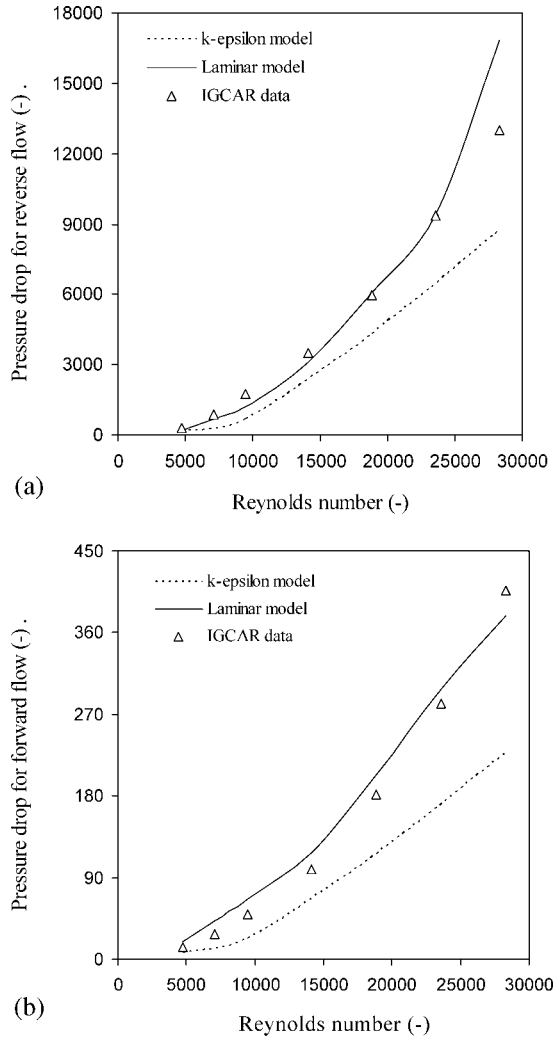

Figure 5. Plot of ΔP_r vs. Re for laminar and standard k-ε model for (a) reverse flow, and (b) forward flow situation.

Simulation results of vortex diode

Comparison with the Experimental Diodicity Values. The experiments for the measurement of pressure drop across six different diode sizes ($d \sim$ 30 mm, 70 mm, 90 mm, 100 mm, 125 mm, and 150 mm) for different flow rates and modes (forward and reverse flow) were carried out. The geometrical details of the diodes are given in Table 1. The details of the experimental setup and the experiments can be seen in Kulkarni et al.[26] For the diodes under consideration the aspect ratio ($\alpha = d/h$) was in the range of 4 to 6, where h is the height of diode chamber. For the experiments carried out to assess the effect of nozzle configuration, diodes of 125 and 150 mm dia. were used with two tangential diffuser nozzles of 25 mm and 20 mm entry diameters. The smaller diameters of diffuser sections are attached to the chamber and for all the diffuser sections of the nozzles; the angle of divergence was maintained constant (5°). In almost all the simulations (except those for analyzing the effect of nozzle configuration), the axial and the tangential nozzles were of the same diameter as the diode height (h).

On selection of the suitable grid size, discretization schemes, gradient options, etc., the flow was simulated for the vortex diodes having 30 mm, 70 mm, 100 mm, 125 mm and 150 mm dia. at four different inlet velocity values. In all the simulations area weighted average pressure was monitored at the inlet and outlet ports, and the respective values of pressure-drop were estimated on convergence of the simulations (residue $<10^{-4}$). As mentioned previously, the estimated pressure-drop data was used for calculating the respective Euler number in forward Eu_f, and reverse Eu_r directions. The diodicity values were obtained from the ratio Eu_r/Eu_f, and its variation with Re was observed and compared with the experimental data.

Figure 6 shows the variation in the experimental and simulated Eu for forward, as well as reverse flow conditions in 30 mm, 70 mm, 125 mm, and 150 mm diodes. For the smaller diode (30 mm), the deviation in Eu_r was seen to have a

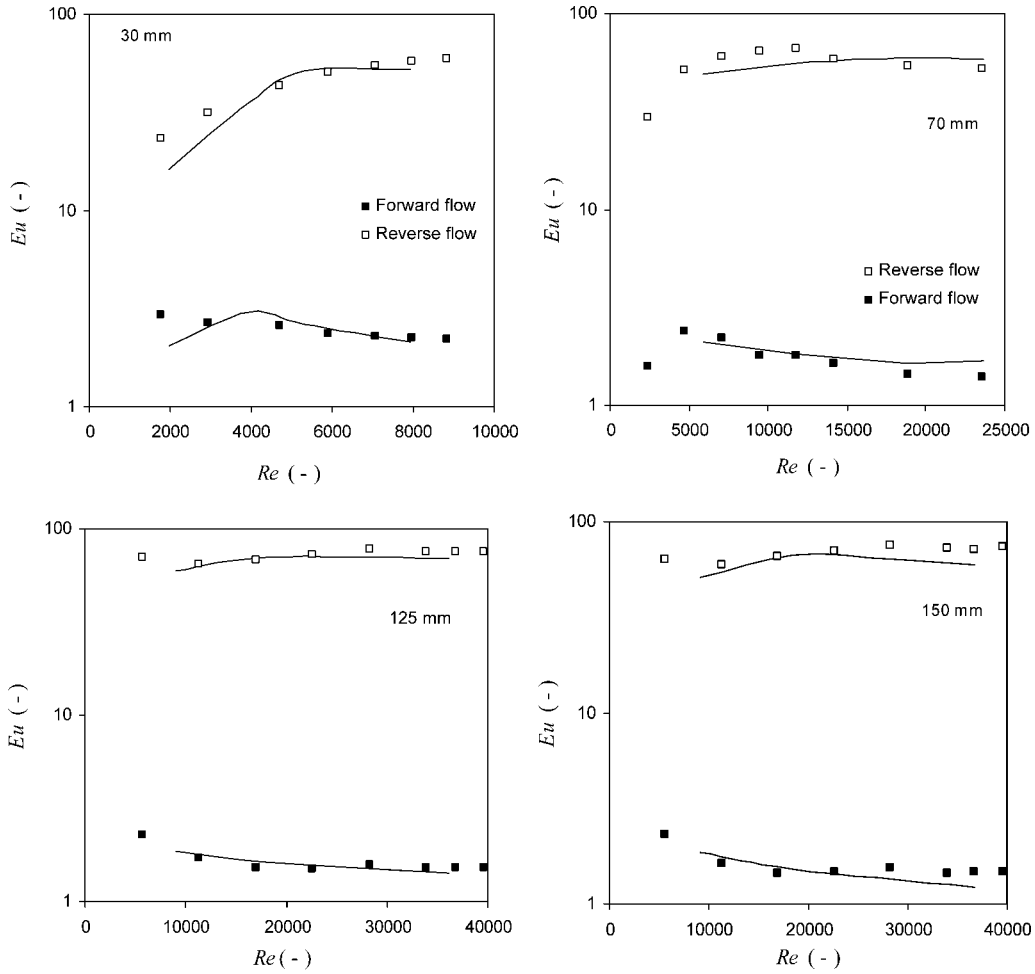

Figure 6. Comparison of simulated estimated Euler number for forward and reverse flow for 30 mm, 70 mm, 125 mm, 150 mm dia. diode at different inlet velocities.

positive dependence on the inlet fluid velocity. On plotting the diodicity from the experiments and simulations, a good agreement between the two was seen (Figure 7) for all the five diodes under consideration. This showed that the selected simulation parameters and the simulation strategy were able to predict the performance of diodes over a wide size and velocity range. It may be noted that the extent of difference between the simulated and the experimental values of Eu (not clearly visible as both Eu_r and Eu_f are plotted on the same graph), and that of the diodicity are of similar order. On satisfactory illustration of the simulation strategy, and satisfactory comparison between the predicted pressure-drop values and the experimental data, now we discuss the simulated flow pattern inside the diode geometry for different diode sizes, and also for other configurational changes like nozzle design, nozzle combination, etc.

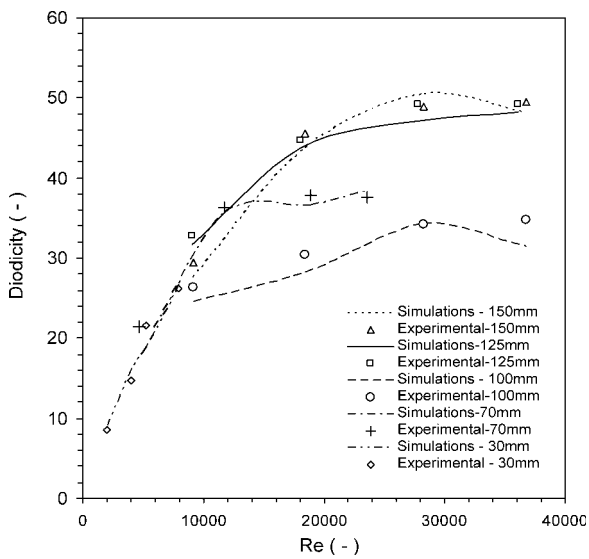

Figure 7. Comparison of the experimental and predicted diodicity values for 30 mm, 70 mm, 100 mm, 125 mm, and 150 mm size diodes.

Simulated flow inside a vortex diode

Knowledge of three-dimensional (3-D) flow fields in the diode chamber would help in understanding the key factors controlling the performance of the diode. These results are

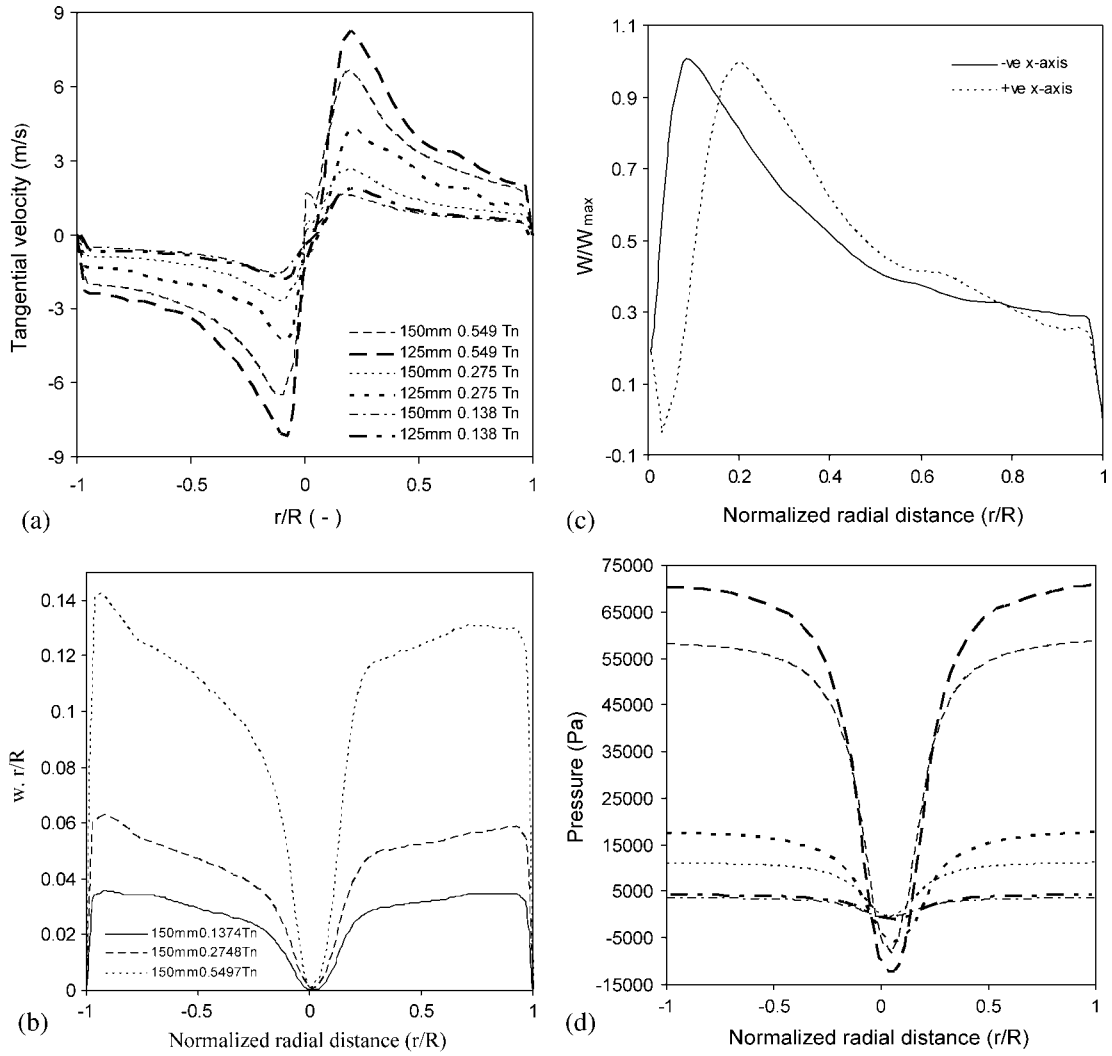

Figure 8. (a) Variation of tangential velocity over the chamber cross-section (along x-axis) for two diode sizes, (b) free and forced vortex regions on both half sections of vortex diode chamber, (c) typical variation of w/w_{max} along the radius of chamber for the case of tangential flow entry at Q = 2600 L/hr, ϕ = 125 mm, and (d) pressure profiles in the diode chamber (along x-axis) for two different diode sizes at three inlet velocities.

Tn in legend indicates the reverse flow (with reference to coordinates in Figure 1a). Legends are same as given in A.

discussed in the following for reverse, as well as forward flow modes.

Reverse Flow. In the reverse flow condition, the fluid enters the diode through tangential entry port, and leaves from the axial port. The tangential nozzle has a converging section toward joining with the diode chamber, which causes continuous increase in the fluid velocity and decrease in the pressure. The tangential entry helps in setting a vortex in the chamber, which had a laminar flow condition in most of its region. Second, in the vortical flow, the tangential component is dominant, and the tangential velocity increases toward the center of the chamber. However, increase in the velocity is not continuous, and it reaches a point (let us call it as the "point of vortex transition"), after which the tangential velocity is proportional to the radius of the chamber. The region where the tangential velocity is proportional to the radius is called forced vortex, while the region where the circulation ($\psi = w \cdot r$) is constant over the radius is called free vortex. CFD simulations were able to capture these two regions for all the inlet velocity conditions and all diode sizes. Figure 8a shows the tangential profiles for 125 mm and 150 mm diodes at three different velocities (0.137, 0.27, 0.549 m/s).

For a 150 mm diode operating in reverse flow condition, the plot of ψ along the chamber diameter (Figure 8b) showed identical behavior at three different inlet velocities. The free vortex region, and the forced vortex regions in the two different half-sections of diode were analyzed separately. Figure 8c shows the point where the vortex transition occurs is different for the half section with the tangential port attachment, and the remaining half section of the chamber. Pressure profiles inside the chamber are shown in Figure 8d, and the pressure was found to decrease continuously toward the center of the chamber. At a constant inlet velocity, smaller diode

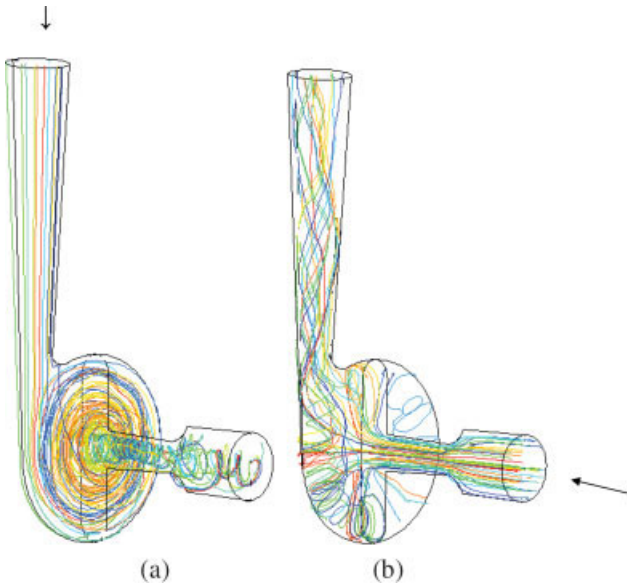

Figure 9. Typical pathlines of the fluid in a 125 mm vortex diode at inlet velocity of 0.423 m/s for the case of (a) reverse flow, and (b) forward flow situations.

Arrows indicate the inlet flow direction. [Color figure can be viewed in the online issue, which is available at www.interscience.wiley.com.]

yielded larger average pressure over the cross-section. The fluid path lines for the fluid for reverse flow, as well as forward flow situations were tracked and are shown in Figure 9. The reverse flow path lines (Figure 9a) show the vortical structure wherein the fluid in the vortex is brought to the center after several rotations over the chamber radius. These path lines also show that not all the fluid elements travel the same distance before it reaches the chamber exit. This illustrates the effect of position of the fluid element in the tangential nozzle at the entrance of the chamber. Second, the axial co-ordinate of the fluid element (i.e., along the chamber height) more or less remains the same during the complete circulation of the fluid.

The vector plot of tangential velocity (not shown here) showed the vortical motion in the chamber that continues to have a significant angular velocity even at the axial outlet. The enlarged view of the vector plot in the region, where the tangential nozzle is attached to the chamber showed that most of the fluid elements are pulled toward the periphery of the chamber indicating a strong tangential vortex, which remains confined right upto the chamber periphery. Further, such a motion also indicates that the transition from the strong axial component in the nozzle to strong tangential component is relatively easy, as the nozzle is attached to the chamber tangentially along its periphery. Later, at the center of vortex, the axial component becomes dominant yet a stronger tangential motion could be seen getting extended even in the axial nozzle from where it exits the chamber. The simulated contour plots for the tangential velocity, and the pressure across the diode cross-section are shown in Figure 10a and 10b, respectively. The pressure distribution and also the tangential velocity distribution over the chamber cross-section show the existence of asymmetry, because of the design of diode (single tangential inlet). Typically the tangential velocity inside of a vortical flow gets stronger towards the eye of the vortex. For the case of reverse flow in a vortex diode, the axial nozzle does not allow the vortex to form an eye, and, hence, the strong tangential velocities remain restricted only up to the region of diode connected to the axial nozzle. It would be important to mention that the unsteady simulations (discussed earlier) of the reverse flow situation yields a precessing vortex, and similar to the analy-

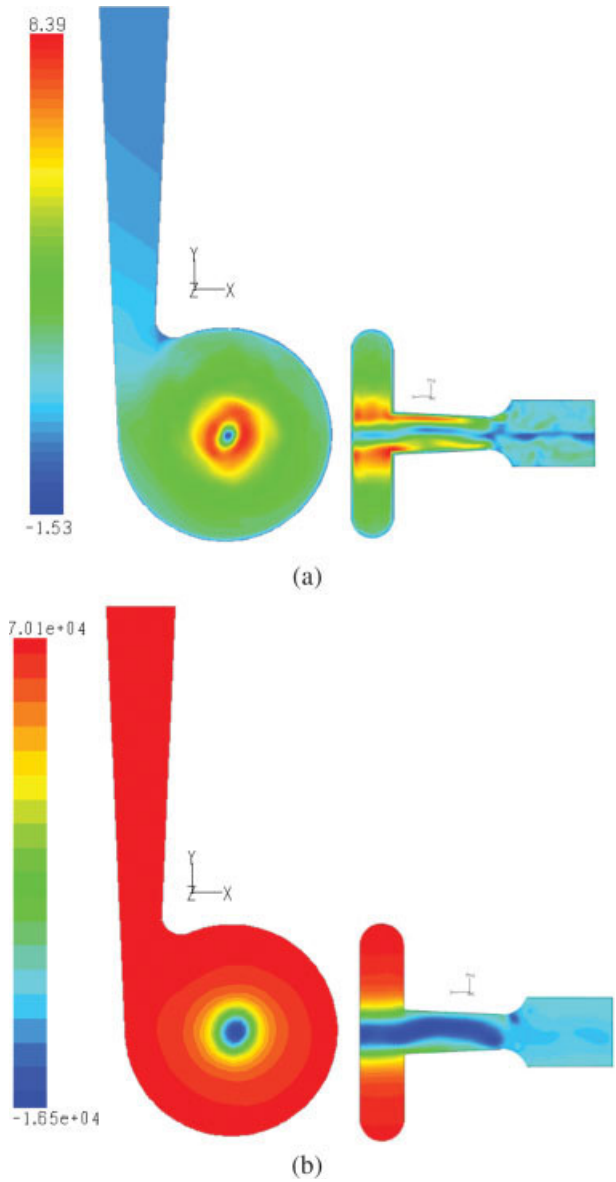

Figure 10. Contour plots from the simulations for reverse flow at Q = 2600 L/hr, in 125 mm diode.

(a) Tangential velocity, the color scale shows the velocity values in m/s, and (b) static pressure, the color scale shows the pressure in Pa. [Color figure can be viewed in the online issue, which is available at www.interscience.wiley.com.]

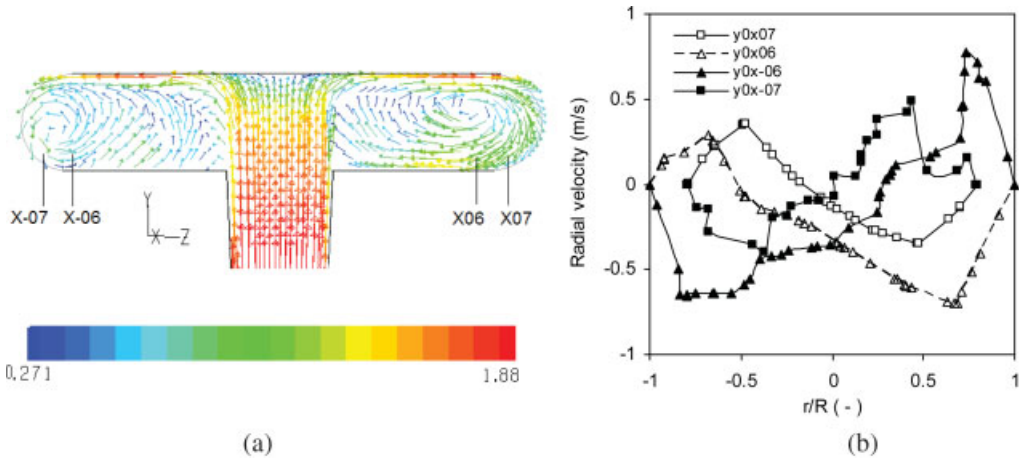

Figure 11. (a) Vector plot for the case of forward flow in the plane Y = 0, and (b) profiles of radial velocity component in the 125 mm diode chamber (along z axis in the plane Y = 0) at different x positions shown in A at Q = 1300 L/hr.

The legends show four different sections for the case of forwards flow (with reference to co-ordinates in Figure 1). [Color figure can be viewed in the online issue, which is available at www.interscience.wiley.com]

sis by Alekseenko et al.[27] the frequency of precession was seen to increase with the inlet flow *Re*.

Forward Flow. When the fluid enters the chamber from its axial entry port, the axial velocity decreases continuously toward the chamber wall facing the axial nozzle (not shown here). The simulations for 125 mm and 150 mm diode showed that the axial velocity for the larger diode was higher at all the cross-sections of the chamber. The vector plot of the chamber in the plane Y = 0 i.e., X-Z plane shown in Figure 11a indicates the formation of a circulatory flow in the region close to chamber periphery. The profiles of radial velocity component at different radial positions along the chamber cross-section in ZY plane are shown in Figure 11b. It is apparent that on entering the chamber, fluid hits the flat wall and gets distributed to create a circulatory flow along the chamber periphery further switching to the tangential exit port. This was mainly due to the radial distribution of liquid over the chamber, which subsequently undergoes circulation. It is important to note that the weak peripheral circulations have a net direction toward the tangential nozzle, and, thus, fluid trapped in these weak circulations is slowly brought to the exit. The pressure distribution over the chamber cross-section was also obtained, and it was found that the values of pressure are significantly lower than the case of tangential flow inlet condition. One of the reasons for relatively lower pressure-drop values is the radial distribution of the flow across the chamber. Inducing uniformity in the radial flow would further reduce the effect of asymmetry in the design, and, thus, help in further lowering the values of pressure drop. The path lines for the forward flow are shown in Figure 9b, and it shows that the fluid impinges on the flat wall of the chamber, and then depending on its location of entrance, it either follows a short path leading to the tangential port or get entrapped in the weak circulation along the periphery (shown later in Figure 11a), which due to asymmetry in the design makes the peripheral vortex to move slowly toward the tangential port, thereby, making the entrapped fluid escape the chamber.

Effect of nozzle design

Effect of Diffuser Divergence Angle. The divergence angle of the diffuser sections of the axial and tangential nozzles is also an important parameter that helps in manipulating the diodicity for a given chamber size. In order to understand this effect, simulations were carried out for a 150 mm diode with nozzles having diffuser sections of 5° and 7° divergence angles. The simulated results are shown in Figure 12. It can be seen that for all the inlet velocities, the simulations for the case of larger convergence angle yielded higher diodicity values. The respective *Eu* values for forward and reverse flow were also seen to be higher. For example, for inlet

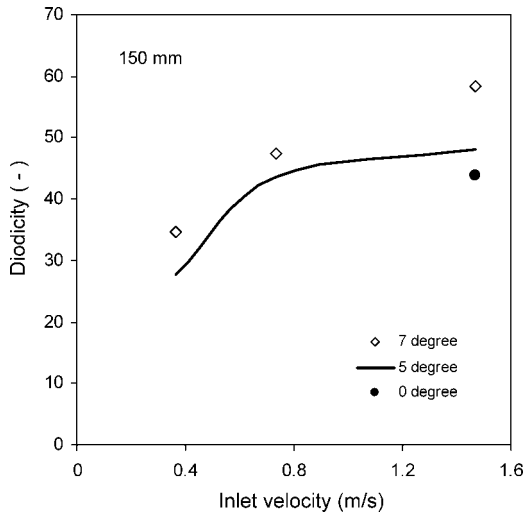

Figure 12. Effect of axial and tangential port divergence angle on the performance of a 150 mm diode.

The inlet velocity is based on the port area connected to the diode chamber.

velocity of 0.55 m/s, Eu_r for 7° angle was higher by 34.67%, while the Eu_f increased by 20.6%, yielding a relatively higher diodicity when compared to the diode with 5° diffuser angles. Additional simulation with both the ports made of straight pipes (0°), which is analogous to the Zobel diode design showed lower diodicity. Although Eu_r for the identical inlet flow rate increased by 34.28% the rise in Eu_f was by 40%, which yielded overall lower diodicity. Thus, on the basis of the earlier analysis, a diode with nozzles having diffuser sections of 7° divergence angle was found to perform better than the other two cases.

Effect of Radius of Curvature for Axial Port. Another parameter related to the nozzles that can also have an effect on the performance of a diode is the radius of curvature (R_C) of the expander portion in the axial nozzle. Figure 13a–b show axial nozzles with expander sections having 16 mm and 32 mm radii of curvature. In both the cases, the angle of convergence for the diffuser sections of both the nozzles was 5°, and the flow was simulated for a 150 mm diode at three different inlet velocities. The estimated diodicity values from these simulations were compared and are shown in Figure 13c. At lower inlet velocities, the diodicity for the case of larger radius of curvature (R_C = 32 mm) was less as compared to the smaller radius (R_C = 16 mm). However, at the inlet velocity of 0.55 m/s, the diodicity for the former was 34% higher than the later. The comparison of the *Eu* for reverse, as well as forward flows for both the diodes as shown in Figure 13d indicates that although the forward flow *Eu* for diode with Rc = 32 mm was higher (by 31%) than that for the case of lower R_C, the extent of improvement in the reverse flow *Eu* was significantly high (76.2%), which yielded a higher diodicity at higher *Re*. At the lowest *Re* under investigation, the increase in forward flow *Eu* was more than that of the reverse flow *Eu* yielding lower diodicity. For the case of inlet velocity = 0.275 m/s, both the *Eu* values showed enhancement in the similar range, thus, yielding no significant variation in the diodicity when compared with the diode with R_C = 16 mm. The analysis shows that the forward flow *Eu* is always higher for the diode with larger R_C, and, thus, the extent of enhancement in the *Eu* in reverse flow situation would decide the relative influence of R_C.

Effect of Diameter of Diffuser Section of Nozzles. Simulations were also carried out to examine the effect of diameter of the diffuser section of the nozzles that is attached to the chamber on the performance of the 125 mm diode. For this case, four different nozzle configurations were tested. Two different axial nozzles (25-20-40.09 mm and 20-16-40.09 mm, where the first, second and the third numbers correspond to the diameter of the port connected to the chamber, the diameter of the diffuser section, and the diameter of the connecting pipe, respectively), and two different tangential nozzles (25–40.09 mm and 20–40.09 mm, where the first and the last numbers correspond to the diameter of the small and the large section of a cone, respectively) were used for getting four combinations. The predicted results are shown in Figure 14 along with the experimental data. It can be seen that the predicted results show qualitative, as well as quantitative agreement with the experimental data. The analysis showed that the nozzles with entry port size equal to height of diode on axial, as well as tangential ports yields maximum diodicity.

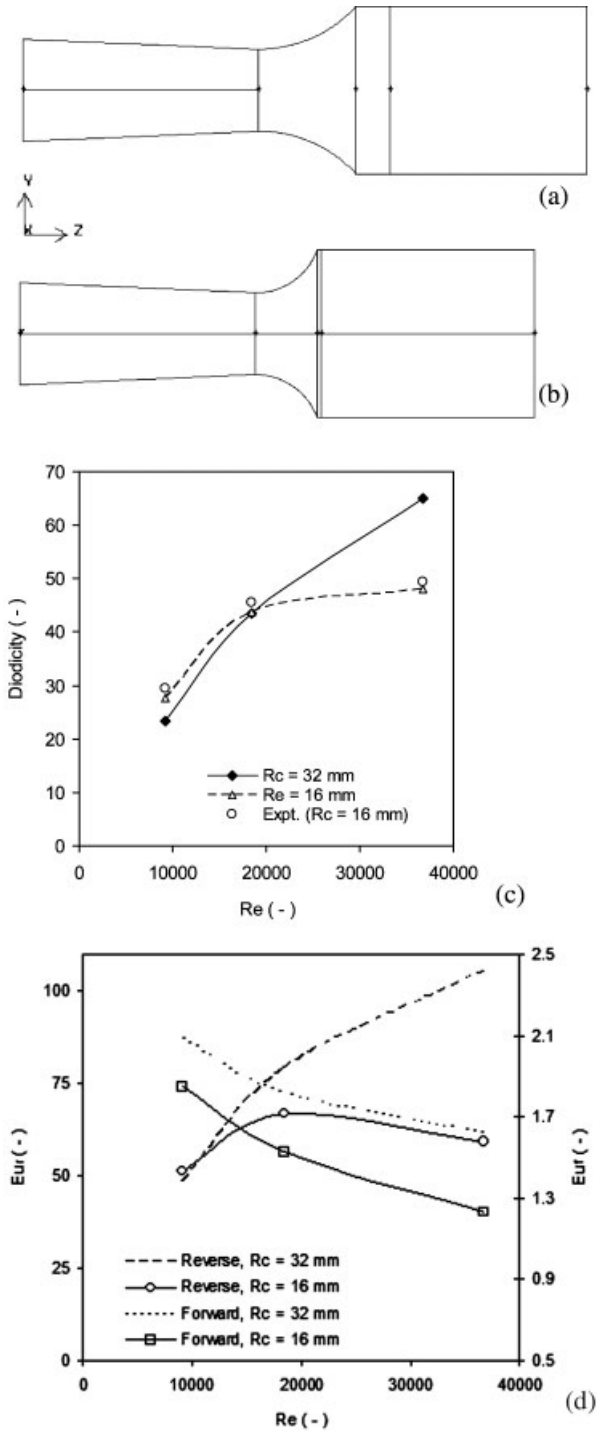

Figure 13. Geometry of the Axial nozzles with (a) 32 mm, and (b) 16 mm radius of curvature for the expander sections, respectively; (c) comparison of diodicity for diodes with axial nozzles having different radius of curvature, and (d) comparison of Eu_f and Eu_r for diodes with axial nozzles having different radius of curvature.

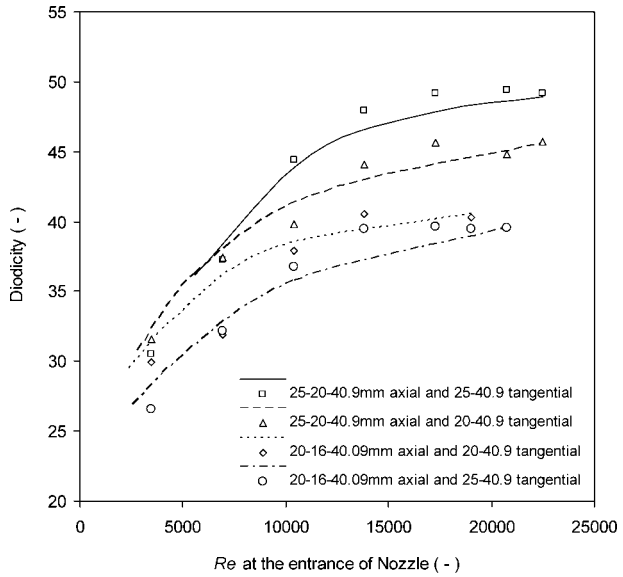

Figure 14. Comparison of the experimental and predicted diodicity values for 125 mm diode with different nozzle configurations.

Lines given in the legends indicate the simulated values for nozzle configuration given against the symbol below it.

The aforementioned discussions bring out certain interesting features of the flow in a vortex diode, and the effect of various design and operational parameters on the same. Further work on measurement of velocity field in the vortex diode, and the spectral analysis of the velocity or pressure fluctuation data in the vortex core would enhance our understanding of flow and performance of vortex diodes. This work is in progress and will be reported later.

Conclusions

CFD simulations of flow through vortex diode were carried out. Influence of simulation parameters was investigated. The predicted results showed good agreement with the experimental data over a range of diode sizes, nozzle sizes and Reynolds number. Key findings of this work are listed in the following:

- Results predicted with the assumption of laminar model showed better agreement with the experimental data indicating the possibility of relaminarization of the flow in vortex diodes.
- The diodicity was seen to increase with Re, and also with the diode size. The variation of diodicity with Re was seen to level-off after certain Re.
- The nozzles with entry port size (portion that is attached to the chamber) equal to height of diode for axial, as well as tangential ports lead to relatively higher diodicity.
- The diodes with 7° angle of convergence for conical sections of nozzles exhibited higher diodicity than that of 5° nozzles.
- The performance of the diode of 150 mm dia., with two different R_c (32 mm and 16 mm) showed different behavior depending on the inlet flow rate. The Eu_f is seen to be always higher for the diode with larger R_c, and, hence, the comparative performance of the diode largely depends upon the extent of enhancement in the Eu_r.

Further experimental verification of some of the predicted results, and further studies on measurement of flow characteristics within diode would help in designing better diodes.

Notation

BLC* = modified boundary layer coefficient
d = chamber diameter, m
d_A, d_T = nozzle diameter where it is attached to the chamber
D = diodicity
D_{Rec} = diodicity at Re_c
Eu = Euler number $\Delta P/(0.5 \cdot \rho \cdot v^2)$
f = friction factor for the flow
g = gravity
p = pressure, Pa
ΔP = pressure drop, Pa
R_C = radius of curvature of the expander section, mm
Re = Reynolds number $Re = d\ v\ \rho/\mu$, $Re = \upsilon_i h/2v$
Re_c = critical Reynolds number
S = swirl number $S = w_i/\upsilon_i$
U = local mean velocity, m/s

Greek letters

α = aspect ratio (ratio of diameter to height of diode)
Γ = circulation, m^2/s
μ = fluid viscosity, kg/m/s
ρ = fluid density, kg/m^3
v = fluid velocity, m/s
v_A = inlet fluid velocity at d_A m/s
υ_i = the value of radial velocity υ at $r = R$
w = swirl component of velocity, m/s

Subscript

A = axial
c = critical
E = expander
f = forward
r = reverse
T = tangential

Literature Cited

1. Escudier MP, Bornstein J, Zehnder, N. Observations and LDA measurements of confined turbulent vortex flow. *J Fluid Mech*. 1980; 98:49–63.
2. Escudier MP, Bornstein J, Maxworthy T. The dynamics of confined vortices. *Proc Royal Soc London A*. 1982;382:335–360.
3. Derksen JJ. Simulations of confined turbulent vortex flow. *Comp Fluids*. 2005;34(3):301–318.
4. Solero G, Coghe A. Experimental fluid dynamic characterization of a cyclone chamber. *Exp Thermal Fluid Sci*. 2002;27:87–96.
5. Peng W, Hoffmann AC, Dries HWA, Regelink MA, Stein LE. Experimental study of the vortex end in centrifugal separators: the nature of the vortex end. *Chem Eng Sci*. 2005;60:6919–6928.
6. Shi L, Bayless DJ, Kremer G, Stuart B. CFD Simulation of the Influence of Temperature and Pressure on the Flow Pattern in Cyclones. *Ind Engl Chem Res*. 2006;45:7667–7672.
7. Hoffmann AC, Stein LE. *Gas Cyclones and Swirl Tubes-Principles, Design and Operation;* Springer-Verlag: Heidelberg, 2002;ISBN 3-540-43326-0.
8. Bradley DL. *The Hydrocyclones*, Paragmon Press, London; 1965.
9. Fernandes EC, Heitor ÆMV, Shtork ÆESI. An analysis of unsteady highly turbulent swirling flow in a model vortex combustor. *Exp in Fluids*. 2006;40:177–187.
10. Priestman GH. A study of vortex throttles Part 2: viscid flow analysis. *Proc Inst Mech Eng*. 1987a;21(C5):337–345
11. Priestman GH. A study of vortex throttles Part 1: Experimental. *Proc Inst Mech Eng*. 1987b;21(C5):331–336

12. Priestman GH, Tippetts JR. Development and potential of power fluidics for process flow control. *Chem Eng Res Des*. 1984;62:67–80.
13. Zobel R. Experiments on a hydraulic reversing elbow. *Mitt Hydr Inst Munich*. 1936;8,1–47 (UKAEA Risley Translation, No. 439).
14. Haakh F. Vortex chamber diodes as throttle devices in pipe systems: Computation of transient flow. *J Hydraulic Res*. 2003;41(1):53–59.
15. Stairmand J. Flow patterns in vortex chambers for nuclear duties. *Nucl Energy*. 1990;29(6):413–418.
16. Wormley DN. An analytical model for incompressible flow in short vortex chambers. *Trans of ASME: J Basic Eng*. 1969;264.
17. Ragab S, Sreedhar M. Numerical simulation of vortices with axial velocity deficits. *Phy Fluids*. 1995;7(3):549.
18. Moin P, Mahesh K. Direct numerical simulation: A tool in turbulence research. *Annu Rev Fluid Mech*. 1998;30:539–78.
19. Ranade VV. Computational Flow Modelling for Chemical Reactor Engineering. Academic Press; New York; 2002.
20. Muntean S, Ruprecht A, Susan-Resiga R. A numerical investigation of the 3d swirling flow in a pipe with, constant diameter. Part 1: Inviscid computation, Workshop On Vortex dominated flows – achievements and open problem. Timisoara, Romania; 2005.
21. Susan-Resiga R, Miloş T, Baya A, Muntean S, Bernad S, Mathematical and numerical models for axisymmetric swirling flows for turbomachinery applications, Workshop on Vortex Dominated Flows Achievements and Open Problems, "Politehnica" University of Timişoara, România, June 10–11, 2005.
22. Deshpande PJ. Study of vortex diode: experiments and CFD modeling. Pune Univ. 2006. ME. Thesis.
23. Narasimha R, Sreenivasan KR. Relaminarization in highly accelerated turbulent boundary layer. *J Fluid Mech*. 1973:61;417–447.
24. Narasimha R, Sreenivasan KR. Relaminarization of fluid flows. *Adv Appl Mech*. 1979;19(221):309.
25. Sreenivasan KR. Laminarescent, relaminarizing, and retransitional flows. *Acta Mech*. 1982;44:148.
26. Kulkarni AA, Ranade VV, Rajeev R, Koganti SB. Vortex Diodes: Some Design Guidelines. *Chem Eng Sci*. 2008.
27. Alekseenko SV, Kuibin PA, Okulov VL, Shtork SI. Helical Vortices In Swirl Flow. *J Fluid Mech*. 1999;382:195–243.

Manuscript received May 23, 2007, and revision received Nov. 23, 2007.